Applied Geomatics
https://doi.org/10.1007/s12518-020-00350-3

ORIGINAL PAPER

Evaluation of the environmental impacts of urbanization from the viewpoint of increased skin temperatures: a case study from Istanbul, Turkey

Behnam Khorrami [1] · Hadi Beygi Heidarlou [2] · Bakhtiar Feizizadeh [3]

Received: 17 August 2020 / Accepted: 24 November 2020

Abstract

Urbanization is an inevitable process all around the world especially in developing countries like Turkey. Istanbul has been experiencing rapid urban expansion for the past 60 years. This urban expansion is leading to the replacement of forests by various artificial surfaces. This situation has a critical impact on the natural surfaces due to the alteration of heat energy balance. In this study, the authors tried to investigate the extent of urbanization of Istanbul within the past decades to unearth its impacts on the urban heat island (UHI) severity and the level of its ecological consequences in terms of decreased thermal comfort. To this end, land use/cover (LULC) and land surface temperature (LST) maps were generated using Landsat imageries based on random forest (RF) classifier (as a machine learning tool) and radiometric image processing algorithms, respectively, for four different dates from 1989 to 2019. The statistical and spectral indicators were calculated for the study area to evaluate the association between urban development and UHI. Results indicate that Istanbul has suffered a continuous land transformation from forest to urban and croplands so that the area of forest has diminished by 373.3 km^2, and the artificial surfaces have increased by 260 km^2. Skin temperatures over all the LULC classes show an increase during the study period with the highest values estimated over artificial surfaces. The statistical analysis of urbanization indicators (ULI, PD, UGSI, NDVI, and NDBI) and UHI indicator (UTFVI) resulted in good correlation coefficients with the best agreement found between NDBI and UTFVI which stresses the strong link between the expansion of built-up areas as a result of urbanization and the severity of UHI and its ecological impacts in Istanbul. Thus, it is a must for policy-makers and officials of the city to take accurate measures regarding the urban planning to mitigate the harsh environmental impacts of growing urbanization of Istanbul in upcoming years.

Keywords Urban development · LST · Random Forest · Urban heat island · Istanbul

Introduction

Urbanization is a common inevitable process in the current world especially in developing countries with a swift growth pace where 90% of the urban growth has occurred (Alfraihat et al., 2016). More than 50% of the world's population lives in cities (Li et al., 2011), and it is expected that by 2050, that number will reach 66% which corresponds to 5 billion people. The most evident consequence of the population growth and urban development is land cover changes (LCCs). A total of 100 M km^2 of the ice-free surfaces have been affected by human activities from which between 23 and 38 M km^2 has been purposely converted, mainly by forest clearing for urban development and croplands (Luyssaert et al. 2014). The transformation of vegetated areas into impermeable surfaces during urbanization brings about the change in the microclimate of urban areas leading to increased skin temperatures (Mallick

✉ Behnam Khorrami
behnam.khorrami@ogr.deu.edu.tr

Hadi Beygi Heidarlou
h.beygi@urmia.ac.ir

Bakhtiar Feizizadeh
feizizadeh@tabrizu.ac.ir

[1] Department of GIS, The Graduate School of Applied and Natural Sciences, Dokuz Eylul University, Doğuş Cad. 207/A Tınaztepe Yerleşkesi, 35390 Buca, Izmir, Turkey

[2] Department of Forestry, Faculty of Agriculture and Natural Resources, Urmia University, Urmia, Iran

[3] Department of GIS and Remote Sensing, Faculty of Planning and Environmental Sciences, University of Tabriz, Tabriz, Iran

Published online: 06 January 2021

et al. 2008; Pal and Ziaul 2017; Pal and Akoma 2009; Beygi Heidarlou et al. 2020) which alters the level of thermal comfort of the residents. Along with other sorts of pollutants, land surface temperature (LST) will rise at a rapid rate which will lead to the detriment of approximately 69% of the world's population by 2050 (United Nations 2010). Urban heat islands (UHIs) are created by rising heat storage capacity of artificial, built-up areas, and urban surfaces, in which this land uses much warmer than rural and natural areas (Rizwan et al. 2008; Tran et al. 2017, Khorrami and Gunduz, 2020). This point-to-point differences in temperatures create a significant effect on people's livelihood and environmental consistency because it deteriorates air quality and people's health and increases energy consumption (Meineke et al. 2014; Plocoste et al. 2014). UHI intensity is related to pattern of LCCs, e.g., composition, structure, and dynamics of forest ecosystems, water and built-up areas, and their changes (Grover and Singh 2015).

Advances in thermal infrared remote sensing (RS), geographic information system (GIS), and statistical analysis have enabled the researchers to describe and study UHI versus vegetative areas and rapid environmental changes (Grover and Singh 2015; Tran et al. 2017). Many studies regarding UHI evaluation have been carried out (Chen et al. 2006; Zhang et al. 2013; Kotharkar and Surawar 2016; Chen et al. 2019; Dissanayake et al. 2019; Ren et al. 2019; Elliot et al. 2020). LST derived from RS satellite data is a special origin of information to define UHIs, and it has been widely used as an index for UHI analyses (Imhoff et al. 2010). With the introduction of thermal RS, LST data is available from a series of satellite sensors (such as ASTER, AVHRR, GOES, Landsat, MODIS, and Sentinel) (Li and Becker 1993; Sun et al. 2007; Wang and Liang 2009; Hulley and Hook 2010; Sobrino et al. 2016; Lemus-Canovas et al. 2020) that cover a wide range of the earth's surface. Thermal imagery provides full spatial coverage at spatiotemporal scales in comparison with air temperature data collected from in situ weather stations on the earth surface (Myint et al. 2013). The research methodologies mainly focus on the changes in land cover and associated LST changes. Surface temperature also has a direct interaction with land use/cover characteristics (Carlson and Arthur 2000). The studies show that there is a strong relationship between the LST and land cover (Amiri et al. 2009), and the analysis of the relationship between them is crucial in order to understand the effects of LCCs on UHI.

LCC is the response to urbanization, where the natural vegetation areas (like forests and rangelands) are replaced by croplands, built-up areas, and impervious surfaces that intensify UHIs (Chun and Guldmann 2014; Kuang et al. 2014; Beygi Heidarlou et al. 2019). Acceleration of urbanization is very high both in intensity and areal coverage in developing countries like Turkey. As a result of rapid population growth and unexpected urban expansion in Istanbul, dramatic LCCs have occurred especially within the past 60 years (Cakir et al. 2008; Geymen and Baz 2008; Balçik 2014). Massive building campaigns and rapid destruction of forests has had a notable impact on the environment and the microclimate of Istanbul (Karaburun et al. 2010). The intense urbanization and dense building construction will finally result in an urban heat island effect with huge temperature differences between urban and rural areas (Balçik 2014). The main objective of the current study is to evaluate the ecological impacts of the UHI over Istanbul regarding the land deformation throughout the past 30 years based on a remote sensing approach.

Study area and dataset

Located in north-west Turkey, the megacity of Istanbul is partitioned into two European and Asian sections by the strait of Bosphorus which connects the Black Sea in the north to the Sea of Marmara in the south of the city (Fig. 1). The climate of Istanbul is moderate (Sensoy et al. 2008) with an annual mean temperature and total precipitation amount of 14.5 C and 677.2 mm, respectively (TSMS, 2020).

Istanbul province has a key role in the industry and politics of the country hosting the largest commercial sectors of Turkey. It attracts a large proportion of the population from all around the country as well as abroad due to its appealing characteristics leading to the fast growth of population and industrialization of the area. The population of the city has increased dramatically from 5,842,985 in 1985 to above 15,000,000 in 2018 (Tarakyanet, 2019). This fast increase of population has led to the very fast development of the city so that the area of the artificial surfaces has increased very much due to the growth of the city and urbanization to the detriment of the city environment and its microclimate. Figure 2 shows the trend of the Istanbul population growth along with the total population of the country. Istanbul metropolitan area plays a preponderant role in the politics and economy of Turkey, the fact that binds the policy-makers to take serious considerations regarding the environmental consequences of the development plans devised and implemented in the area.

To carry out the current study, two data types were used: the population data were obtained from the Turkish Statistical Institute (TSI), and remotely sensed imageries of Landsat satellite series TM5 and $ETM^{+}7$ in 4 different periods were downloaded from USGS online database. Landsat Level 2 imageries are atmospherically corrected accompanied by various remotely sensed products such as surface reflectance, spectral indices, etc. In the current study, Landsat L2 imageries were used to refrain from extra atmospheric correction practices. The study area is scanned completely in two nearby scan rows (031 and 032) so imageries were selected from two scan lines. Table 1 shows the details of satellite images employed in current research.

Fig. 1 The geographical location of Istanbul province (NW Turkey) with the spatial distribution of the meteorological stations used in the study

RFML for LULC mapping

Random forest (RF) is a popular ensemble classification method in which a set of classifiers (trees) are established through learning algorithms (Akar and Gungor, 2012). Each classifier is generated based on a random vector independently assigning a unique vote to the majority class for the classification of the input vector (Breiman 1999, Pal 2005). The classification is done by the increased diversity between classification trees (Naghibi et al., 2016) through resampling the original training dataset (N) with replacement. Image pixels are classified according to the highest vote achieved for the trees of the forest (Breiman 1999).

In this study, the training data (200 points for each type of land use/cover) for the interested classes (forest, croplands, water bodies, and artificial surfaces) of land use/cover (LULC of the study area were collected via visual interpretation of Landsat imageries (Song et al., 2015), then land cover attribution of each point was verified using high-resolution imagery in Google Earth (Baumann et al., 2015, Beygi Heidarlou et al. 2020). These training data were used to classify Landsat images using a nonparametric random forest

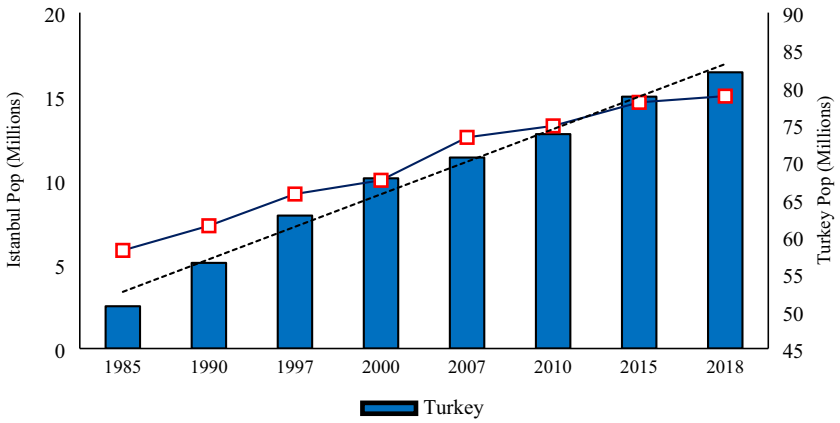

Fig. 2 National census statistics indicating the population development from 1985 to 2018 in turkey and istanbul

Table 1 Characteristics of the satellite imageries used in the study

	1989		2001		2011		2019	
Imaging date	26 Jun ™ 5		11 Jun ™ 5		23 Jun ™ 5		07 Jul $^{E_{TM+}}$	
Path/row	180/031	180/032	180/031	180/032	180/031	180/032	180/031	180/032
Center Lat	41.761	40.330	41.773	40.338	41.763	40.332	41.766	40.338
Center Long	29.117	28.653	29.037	28.573	29.088	28.626	29.021	28.562

classifier. For post-processing of the classified imageries, an iterative majority filter with a 3 × 3 kernel size was applied (Coulter et al., 2016, Beygi Heidarlou et al. 2019).

Thematic accuracy assessments of LULC maps calculated using confusion matrices (Tsendbazar et al., 2016) based on the stratified random sampling of 40 points for each class and high-resolution imagery interpretation in Google Earth (Baumann et al., 2012). The area-weighted accuracy assessment and class-specific accuracies were then calculated using the method described by Olofsson et al. (2013). The variance and confidence level of the accuracies were derived using the equations for stratified random sampling based on a 95% confidence interval (CI) (Olofsson et al., 2013).

Mapping UHI

Retrieval of skin temperatures

Urban heat island (UHI) is defined as a phenomenon in which there is a thermal field difference between an urban area and the outskirt areas nearby. The ecological impacts of increased skin temperatures are described based on the severity index of UHI. The first step to map the severity of UHI is to derive skin temperatures of the earth. The LST maps of Istanbul were generated as follows:

1. Calculation of the top of atmosphere (TOA) radiance: Landsat raw records (DNs) are converted into a radiance based on the following equation:

$$L\lambda = ML \times QCAL + AL \tag{1}$$

"L_λ" is the spectral radiance of top of the atmosphere, "M_L" and "A_L" are the band-specific multiplicative and additive rescaling factors respectively, and "Q_{CAL}" is the quantized and calibrated standard product pixel values (DN) (Salih et al., 2018).

2. Calculation of the brightness temperature (T_B): calculated radiance bands are converted into brightness temperature:

$$T_B = \frac{K_2}{\ln\left(\frac{K_1}{L_\lambda} + 1\right)} - 273.15 \tag{2}$$

"T_B" is the TOA brightness temperature in Celsius, "L_λ" is the TOA spectral radiance, and "K_1" and "K_2" are band-specific thermal conversion constants (Salih et al., 2018).

3. Estimation of skin temperature:

$$LST = \frac{T_B}{\left[1 + \left(\frac{T_B}{C_2} \times \lambda\right) \times \ln(LSE)\right]} \tag{3}$$

T_B is the brightness temperature in °C, "$C_2 = h \times c / s = 14{,}380$", [$h$ = plank's constant (6.626 × 10–34 JS), s = Boltzmann constant (1.38 × 10–23 J/K), c = velocity of light (2.998 × 10–8 m/s)], λ is the mean wavelength, and LSE is the surface emissivity (Khorrami et al., 2019). The specific coefficients required for the estimation of LST in Eqs. 1 and 2 are given in Table 2.

Table 2 The specific thermal coefficients of Landsat satellites

Parameter	Landsat 5 ™ B6	Landsat 7 $^{E_{TM+}}$ B6
Mean wavelength (λ)	11.45	11.45
K_1	607.76	666.09
K_2	1260.56	1282.71
M_L	5.5375×10^{-2}	3.7205×10^{-2}
A_L	1.18243	3.16280

Table 3 Categorization of the severity of UHI and its ecological impacts according to ranges of UTFVI

Category	UTFVI	UHI severity	Ecological impact
1	< 0	None	Excellent
2	0.000–0.005	Weak	Good
3	0.005–0.010	Middle	Normal
4	0.010–0.015	Strong	Bad
5	0.015–0.020	Stronger	Worse
6	> 0.020	Strongest	Worst

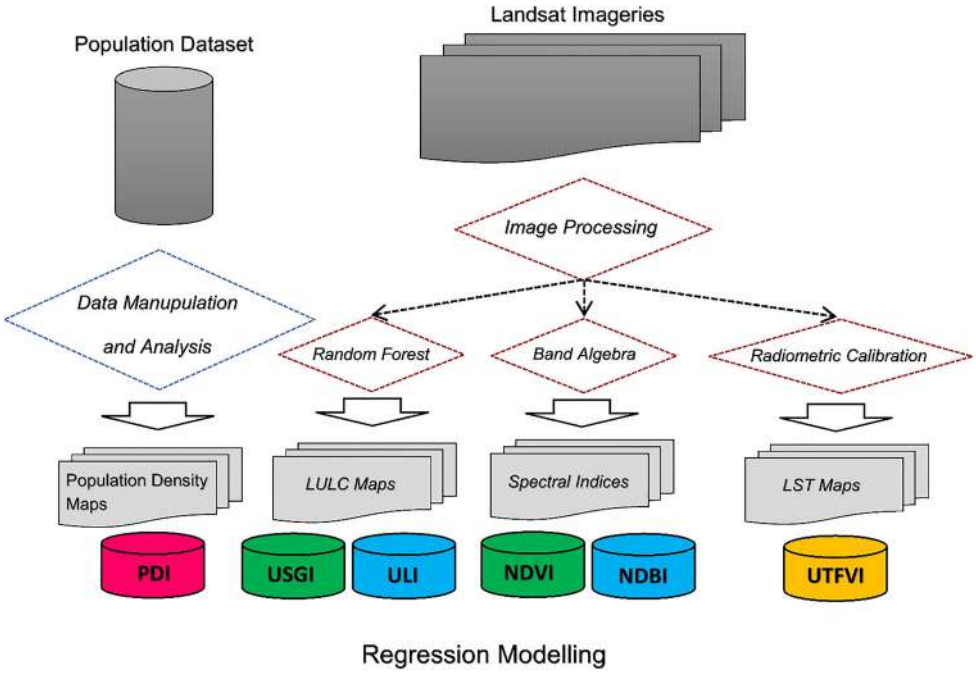

Fig. 3 The graphical flowchart of the methodology

Table 4 Confusion matrices of the land use/cover maps for 1989, 2001, 2011, and 2019. Accuracy measures are presented with a 95% confidence interval

1989		Reference classes				Total	User's	Producer's	Overall
		1	2	3	4				
Map classes	1	39	2	0	6	47	0.83 ± 0.07	0.99 ± 0.01	0.87 ± 0.07
	2	0	33	1	2	36	0.92 ± 0.04	0.48 ± 0.16	
	3	0	1	39	0	40	0.98 ± 0.03	0.54 ± 0.12	
	4	1	4	0	32	37	0.86 ± 0.06	0.69 ± 0.07	
Total		40	40	40	40	160			
2001		Reference classes				Total	User''s	Producer''s	Overall
		1	2	3	4				
Map classes	1	37	2	0	2	41	0.90 ± 0.02	0.99 ± 0.01	0.91 ± 0.03
	2	1	37	2	1	41	0.90 ± 0.03	0.57 ± 0.16	
	3	1	0	38	0	39	0.97 ± 0.01	0.46 ± 0.27	
	4	1	1	0	37	39	0.95 ± 0.02	0.87 ± 0.08	
Total		40	40	40	40	160			
2011		Reference classes				Total	User''s	Producer''s	Overall
		1	2	3	4				
Map classes	1	35	1	0	3	39	0.90 ± 0.03	0.98 ± 0.01	0.86 ± 0.08
	2	2	36	1	1	40	0.90 ± 0.03	0.64 ± 0.16	
	3	1	1	39	2	43	0.91 ± 0.01	0.61 ± 0.19	
	4	2	2	0	34	38	0.89 ± 0.05	0.80 ± 0.08	
Total		40	40	40	40	160			
2019		Reference classes				Total	User''s	Producer''s	Overall
		1	2	3	4				
Map classes	1	34	1	0	5	40	0.85 ± 0.05	0.96 ± 0.01	0.89 ± 0.04
	2	3	35	2	3	43	0.81 ± 0.07	0.62 ± 0.20	
	3	0	2	38	1	41	0.93 ± 0.03	0.53 ± 0.22	
	4	3	2	0	31	36	0.86 ± 0.05	0.70 ± 0.12	
Total		40	40	40	40	160			

1 = forest, 2 = croplands, 3 = artificial surfaces and 4 = water

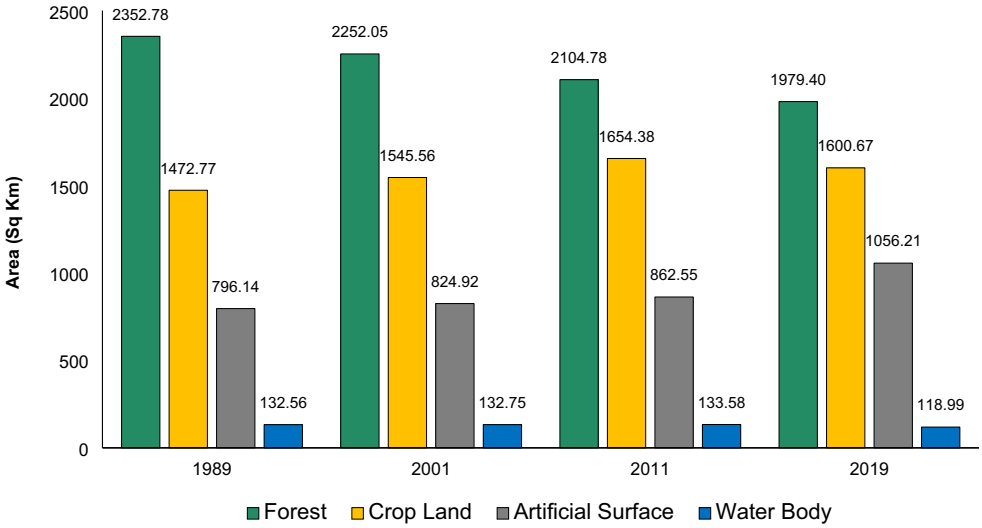

Fig. 4 Temporal statistics of LULC Variations

Estimation of the land surface emissivity (LSE) is essential to retrieve LSTs. Because different features on the earth's surface have different emissivity, the calculation of LSE is quite complicated. Here, the NDVI-based emissivity approach was used. In this approach, the surface emissivity values are estimated based on the fractional vegetation cover (FVC) and typical emissivity values (0.99 and 0.97 for vegetated and non-vegetated surfaces respectively) (Parastatidis et al., 2017). The FVC is estimated under the assumption that the NDVI threshold for non-vegetated and vegetated surfaces is 0.18 and 0.85, respectively (Parastatidis et al., 2017). The following equations were used to estimate LSE:

$$\mathrm{LSE} = \varepsilon_{\mathrm{NonVeg}} \times (1-\mathrm{FVC}) + \varepsilon_{\mathrm{Veg}} \times \mathrm{FVC} \tag{4}$$

$$\mathrm{FVC} = \left[\frac{\mathrm{NDVI}-\mathrm{NDVI}_{(\mathrm{NonVeg})}}{\mathrm{NDVI}(\mathrm{Veg})-\mathrm{NDVI}_{(\mathrm{NonVeg})}}\right]^2 \tag{5}$$

$$\mathrm{NDVI} = \frac{NIR-R}{NIR+R} \tag{6}$$

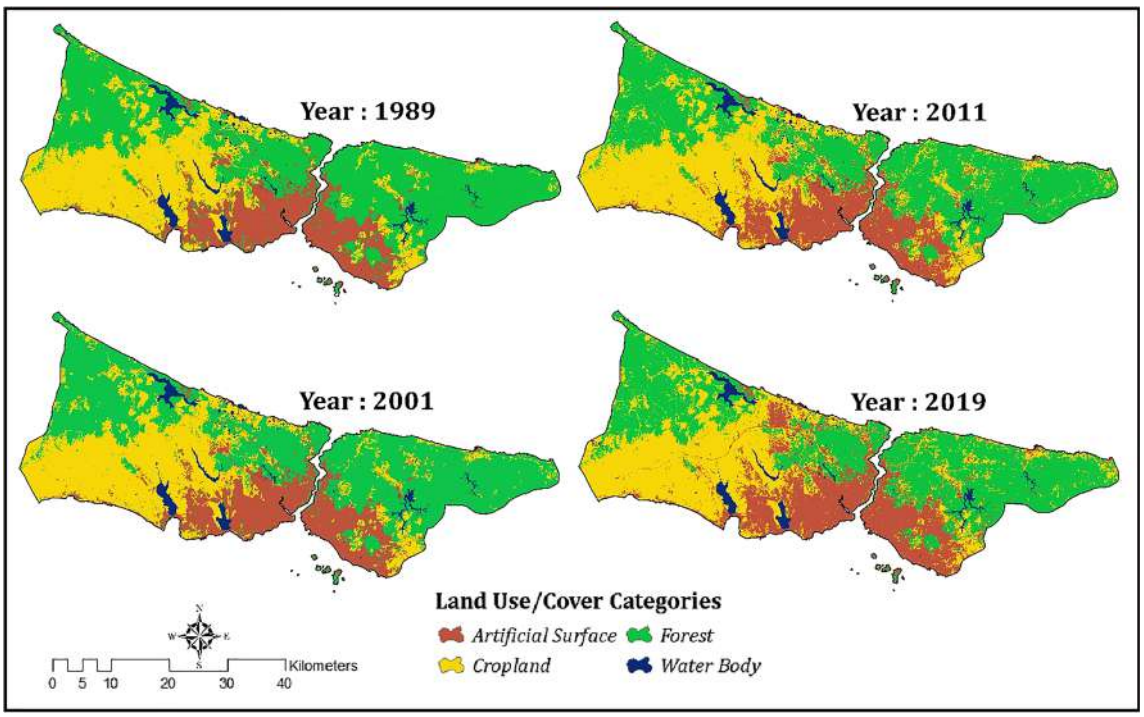

Fig. 5 The spatial maps of land use/cover of Istanbul

Table 5 The results of ground-based validation of skin temperatures

Station ID	Name	June 1989		June 2001		June 2011		July 2019		*R*
		MDT	LST	MDT	LST	MDT	LST	MDT	LST	
17636	Flora	24.00	26.68	22.20	28.79	23.70	27.95	26.40	29.20	0.25
17060	Ataturk Airport	19.80	30.84	23.80	33.69	24.40	31.67	27.10	32.14	0.45
17062	Kadikoy Rihtim	24.60	27.52	23.00	29.20	23.70	30.44	26.60	32.40	0.58
17061	SARIYER	21.40	21.95	19.90	24.99	22.30	23.69	24.50	25.65	0.34
17059	Kumkoy	20.80	24.12	18.90	24.99	19.70	24.99	24.10	27.85	0.83
17610	Sile	20.90	23.26	19.10	25.84	22.30	24.13	23.50	28.39	0.40

Calculation of UTFVI

There are different approaches in detecting the UHI phenomenon based on the statistical variations of the thermal characteristics between urban and rural areas (Khorrami and Gunduz, 2020). One of the most common ways to calculate the severity of UHI and to express its ecological impacts is urban thermal field variance index (UTFVI) (Wang et al. 2018). Using the following equation (Eq. 7), the area of interest is categorized into 6 different classes of thermal severity (Table 3) based on the amount of UTFVI (Renard et al. 2019) which ranges between less than 0 (the least ecological impact) to more than 0.02 (the worst ecological impact):

$$\mathrm{UTFVI} = \frac{(T_s - T_{\mathrm{mean}})}{T_s} \tag{7}$$

where T_s and T_{mean}, represent the surface temperature of a point of interest in the area and the mean surface temperature of the whole area respectively.

Investigation of the urban development

The urbanization process and its extent can be studied through a variety of statistical as well as spectral metrics. Spectral characteristics of the land surface features define the way they appear on satellite imageries. Any change in the quality and quantity of the features can be detected based on their footprints left on the spectral domain of the imageries using image-processing techniques. Spectral indices are widely used in remote sensing to monitor the variations of land surface features. These indices are a combination of different bands generated based on specific formulas defined according to the spectral response of a feature. Urbanization is linked with tangible changes in land surface features including the increase of artificial surfaces and a decrease of green spaces as a result of population growth. In the current study, the urban development rate of Istanbul was studied using the following important indicators:

PD From the fact that any urbanization activity is in direct relation with population influx to the area, the development of urban areas in time and space can be evaluated based on the population density. Population density has been applied as the sole indicator of urban development in several studies because of the ease of its calculation (Ewing and Chen, 2002). Urban areas are defined based on a specific density threshold for the population of a given area. The functional urban area (FUA) method (OECD, 2018) considers areas with more than 1500 residents per square km as urban areas.

ULI To show the order of urbanization, the urban land index (ULI) defined by Haas (2016) was calculated. ULI is defined as the ratio between the urban land (UL) and the total land (TL) of the study area.

$$\mathrm{ULI} = \frac{UL}{TL} \times 100 \tag{8}$$

NDBI Built-up areas are a combination of the buildings and other man-made features. The volume of the built-up areas increases as a direct result of urbanization. Normalized difference built-up index (NDBI) is a very useful and straightforward spectral index in remote sensing for the detection of and mapping the built-up areas. It is based on the differences between the spectral signature of the built-up features in shortwave infrared (SWIR) and near-infrared (NIR) bands. Built-up areas have higher reflectance in the SWIR range (1.55~1.75 μm) compared with the NIR range (0.76~0.90 μm) of the electromagnetic spectrum (Malik et al., 2019). NDBI ranges from − 1 to + 1 where the higher values indicate the denser areas. It is calculated using the following equation:

$$\mathrm{NDBI} = \frac{SWIR - NIR}{SWIR + NIR} \tag{9}$$

Table 6 Temporal statistics of surface temperature derived for each LULC category

Land use/cover	Year	Area (km^2)	LST statistics			
			Min	Max	Mean	Std
Forest	1989	2353	16.57	36.45	23.39	2.53
	2001	2252	16.57	43.01	26.96	2.68
	2011	2105	12.84	33.69	23.03	1.71
	2019	1979	20.84	36.80	24.41	1.69
Croplands	1989	1473	17.48	37.24	26.77	2.34
	2001	1546	19.74	45.62	32.65	2.71
	2011	1654	13.78	38.04	28.20	1.86
	2019	1601	18.82	42.29	30.83	2.58
Artificial surface	1989	796	17.48	38.40	29.28	2.20
	2001	825	17.94	51.41	33.17	2.38
	2011	863	17.94	43.38	30.32	2.02
	2019	1056	17.93	48.05	32.28	2.34
Water	1989	133	16.11	34.08	21.62	3.07
	2001	133	14.25	38.81	22.36	3.11
	2011	134	17.03	35.68	21.62	1.38
	2019	119	19.39	42.29	23.31	1.53

UGS Green spaces have a determining role in the microclimate of urban areas with a key ecological and environmental function in mitigating the UHI impacts, enhancing the environmental quality and controlling the urban development (Chen et al., 2019; Schell, 2018). Urban green space (UGS) is defined as the urban surface covered by living plants including forests, parks, grasslands, and other green bodies (Steyven et al., 2018). The development of urban areas results in the loss of green spaces inside urban areas. In this study, two indices of NDVI and Urban Green Space Index (UGSI) were used as UGS indicators. The UGSI is calculated according to the ratio of urban green space to the total land at a given time:

$$\mathrm{UGSI} = \frac{UGS}{TL} \times 100 \tag{10}$$

The flowchart of the methodology of the current study (Fig. 3) illustrates the necessary steps to accomplish the study.

Results and discussion

The spatiotemporal variations of LULC

Land surface features have a dynamic nature in terms of continuous changes of the features both in time and in space. Changes in the appearance of the land surface can be resulted by different mechanisms either natural or anthropogenic. One of the most effective factors in land use/cover alteration, especially in recent decades, is human activity. Changes in LULC can be used as an indicator of urbanization. In remote sensing of the environment, and the LULC changes are categorized and monitored using a variety of satellite imageries based on different techniques. In the current study, the spatiotemporal status of the LULC in Istanbul was evaluated based on the random forest (RF) algorithm. The accuracy assessment of the classification was implemented using confusion matrices (Table 4). The overall precision with the min accuracy of 0.86 indicates the suitability of the RF classifier algorithm thus the accuracy of the LULC maps generated for the study area.

Figures 3 and 4 show the variations of LULC of Istanbul. According to the results, from 1989 to 2019, a descending trend with a total loss of 373.3 km^2 in the forest cover is seen while the area of croplands and artificial surfaces show an increase with 128 km^2 and 260 km^2 respectively. The LULC maps in Fig. 4 show the position and the geographical variations of the land surface classes. According to these maps, the mid-southern parts of the province, neighboring the Bosporus strait, have been the center for the residential structures and urbanism throughout the past 30 years. The expansion of the urbanization process is toward the wooded and croplands nearby the current urban areas especially for residential and industrial purposes.

Evaluation of UHI severity

As the first step for the evaluation of the environmental impacts of UHI, the skin temperatures were retrieved from Landsat imageries (Fig. 5). The estimated temperatures were validated in comparison by ground truth records. Field-based measurements are the most reliable data because of the high confidence level they provide for the users; thus, they are widely used as an accurate reference for the validation of remote-sensing products. Unfortunately for the study area, the recorded data of desired variables, such as soil temperature and surface radiation, for validation purposes were not accessible for the study period. From the data received from the Turkish State Meteorological Service (TSMS 2020), the only useable data for the current study were mean daily temperatures (MDTs). Taking into account the fact that estimated skin temperatures may vary from the air temperatures which are gauged at a higher elevation rather than the earth surface, MDT records were used as ground truth data for checking the validity of the satellite-based skin temperature values. Table 5 shows the six meteorological stations with MDT and LST values and the correlation coefficient (at 0.95 level) for each station in the study area. Results indicate a fairly good agreement between the estimated and gauged temperatures for the stations with the best correlation achieved for Kumkoy station.

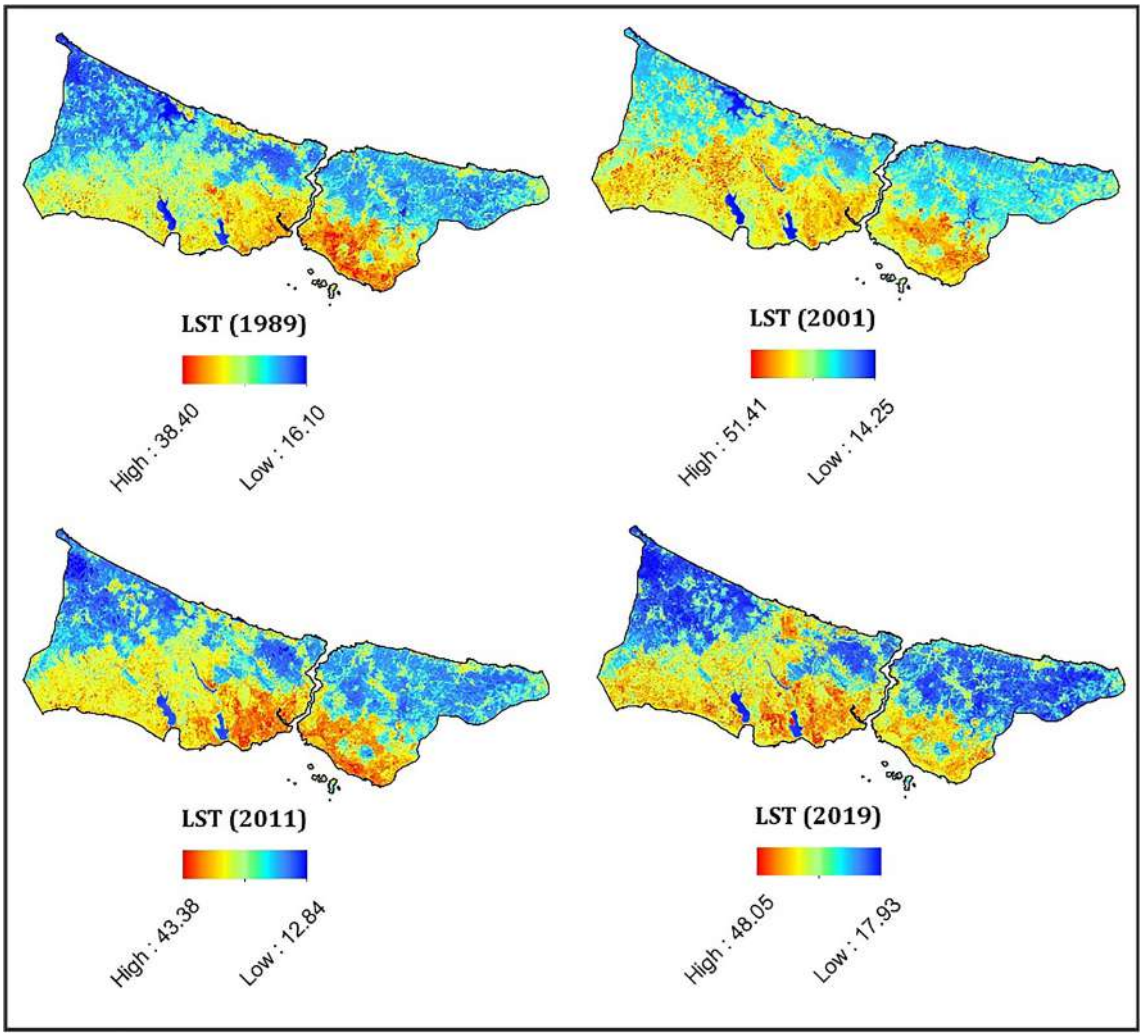

Fig. 6 Spatiotemporal variations of skin temperatures

Summary statistics of the temporal variations of the zonal statistics of skin temperature values for each LULC class is given in Table 6. The temperature values show an increase over all the land covers of the study area. The hot spots concentrate over the artificial surfaces with the max values of temperature while water bodies and wooded lands are the features with the min estimated values of temperature (cold spots).

Table 7 The statistics of the area under each UHI severity class

	Area	1	2	3	4	5	6
1989	km^2	2377.63	719.47	642.72	471.88	379.19	161.87
	%	50.03	15.14	13.52	9.93	7.98	3.41
2001	km^2	2337.17	528.57	522.03	668.75	436.61	259.67
	%	49.17	11.12	10.98	14.07	9.19	5.46
2011	km^2	2337.27	547.44	640.85	694.19	389.28	146.39
	%	49.15	11.51	13.48	14.6	8.19	3.08
2019	km^2	2354.63	420.71	461.75	663.63	562.1	289.9
	%	49.54	8.85	9.72	13.96	11.83	6.1

The thematic maps of the ecological impacts of UHI in terms of severity level over Istanbul were produced using the retrieved LST maps and based on the UTFVI values. For better description of the results, the spatial association of UHI severity and LULC is given in Fig. 6. According to the results, the most severe UHI phenomenon (hot spots) is experienced in urban and constructed areas especially in the vicinity of Bosphorus strait in the downtown, the highly congested areas, while the croplands suffer less. The urban forests have zero severity of UHI which demonstrates the role of vegetated areas in mitigating increased skin temperatures.

The sum of the area under each category is given in Table 7. It is revealed that the area of positive ecological impacts (below normal) has decreased during the study period. While the negative impact (above normal) shows an increase where the worst ecological impact category increased by 2.69% of the total area of Istanbul. The status of the city in 2019 regarding the extent and severity of the UHI is more

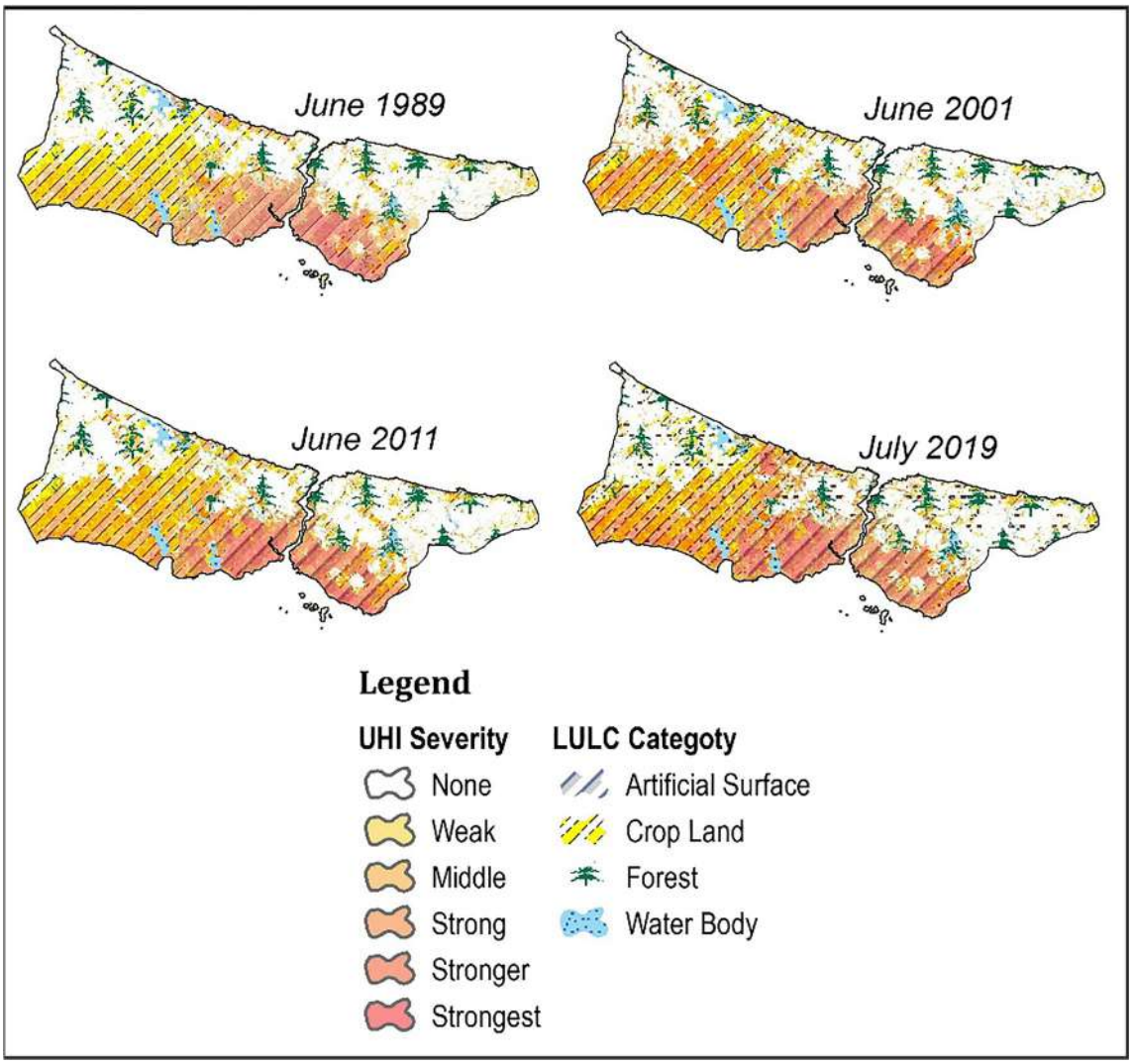

Fig. 7 Spatial interactions of UHI severity and LULC

dramatic in 2001 and 2019 with a total area of 5.46% and 6.1%.

The association between UHI and urbanization

In the current study, for describing the extent of the association between urbanization and UHI severity, the interaction of urbanization indicators including ULI, NDBI, NDVI, UGSI, and population density (PD) with UHI was investigated statistically based on the correlation coefficient values. NDVI and NDBI were calculated spectrally using the desired bands. ULI, UGSI, and PD were calculated statistically using the values derived from LULC maps (for ULI and UGSI) and the population statistics over each zone in the study area. Figures 7 and 8 show the maps of NDVI and NDBI, respectively. The qualitative visual evaluation of the maps suggests an almost complete harmony in the spatial variations of NDVI, NDBI, and UHI severity. The severe ecological impact of UHI corresponds to the areas with low NDVI and high NDBI which approves the theoretical relationship of these indicators.

The correlation coefficients derived for the interacting factors (Table 8) express the strength of the associations between urbanization and the severity of UHI environmental impacts in Istanbul. According to the results, there is a good agreement between urban development and the severity of UHI in Istanbul. The best correlation was found for NDBI and UTFVI for all the dates, which demonstrates the great impact that the development of new built-up areas has on the severity of the UHI and also its impacts. The results of the multiple regression modeling (Table 9) also suggest that out of all the predictive factors of UTFVI over the study area, only NDBI has a statistically significant impact on UHI in Istanbul. That is, the remaining indicators are redundant. Thus, it can be inferred that the urban development in terms of built-up areas controls the severity of UHI over Istanbul.

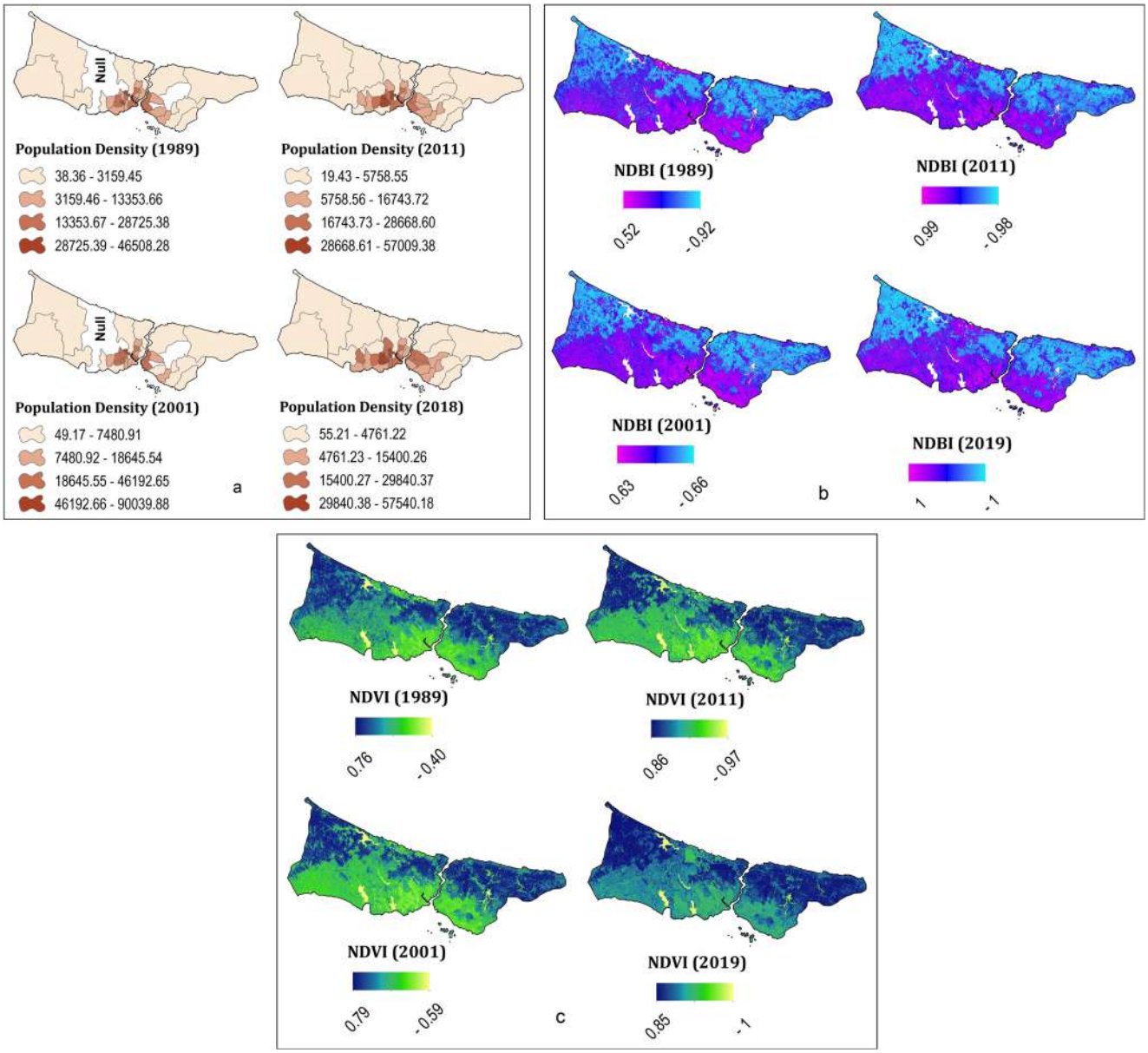

Fig. 8 The spatial illustration of population density (**a**), NDBI (**b**), and NDVI (**c**) in Istanbul

Table 8 The correlation results of the associations of indicators

	UTFVI			
	1989	2001	2011	2019
ULI	0.845	0.755	0.876	0.824
NDBI	0.976	0.917	0.981	0.985
NDVI	− 0.926	− 0.878	− 0.956	− 0.963
UGSI	− 0.836	− 0.842	− 0.934	− 0.605
PD	0.561	0.467	0.715	0.681

Conclusion

Urbanization is an inevitable process especially in the current era with the swift developments in technology and the increased social expectations. The growth of the population requires developing residential as well as the industrial areas to sustain human needs. As a result of population growth, more structures are built up so that the current urban areas start to expand toward the rural areas in the vicinity resulting in the destruction and deformation of the rural nature. During history, all around the world, more and more forests and croplands have been changed into artificial areas. While the primary purpose of urban development is to provide comfort and ease of life

Table 9 Multiple regression analysis results

Model summary

Year	Model	*R*	*R* square	Adjusted *R* square	Std. Error of the Estimate	
1989	1	0.918[a]	0.842	0.812	0.00389	
2001	1	0.927[a]	0.860	0.833	0.00320	
2011	1	0.994[a]	0.988	0.985	0.00098	
2019	1	0.988[a]	0.976	0.971	0.00141	
Coefficients[a]						
Model		Unstandardized coefficients		Standardized coefficients	*t*	Sig.
		B	Std. Error	Beta		
1989	(Constant)	− 0.002	0.007		− 0.236	0.816
	NDBI	0.069	0.022	0.803	3.121	0.000
	NDVI	− 0.019	0.021	− 0.323	− 0.916	0.368
	PD	− 0.148	0.060	− 0.254	− 2.450	0.021
	ULI	8.505E−5	0.000	0.330	1.749	0.092
	GSI	0.000	0.000	0.417	1.984	0.058
2001	(Constant)	− 0.002	0.006		− 0.265	0.793
	NDBI	0.106	0.026	1.398	4.103	0.000
	NDVI	− 0.007	0.020	− 0.147	− 0.365	0.718
	PD	0.021	0.043	0.044	0.479	0.636
	ULI	− 5.240E−5	0.000	− 0.231	− 1.339	0.192
	GSI	0.000	0.000	0.472	1.621	0.117
2011	(Constant)	− 0.005	0.002		− 2.191	0.040
	NDBI	0.077	0.008	0.980	9.246	0.000
	NDVI	0.005	0.006	0.109	0.914	0.372
	PD	0.039	0.050	0.034	0.787	0.440
	LUI	5.906E−5	0.000	0.244	4.257	0.000
	GSI	3.306E−5	0.000	0.115	1.165	0.258
2019	(Constant)	0.010	0.003		2.823	0.010
	NDBI	0.065	0.010	0.842	6.723	0.000
	NDVI	− 0.011	0.007	− 0.190	− 1.485	0.152
	PD	0.070	0.052	0.079	1.348	0.192
	ULI	− 1.795E−5	0.000	− 0.070	− 0.917	0.369
	GSI	2.061E−5	0.000	0.053	1.228	0.233

for the human being, the side effects of this practice are normally taken for granted. The environmental and ecological impacts of LULC alteration may include the increase in energy consumption, change of the urban climate (microclimate) with increased temperatures and emergence of urban heat islands, deterioration of water quality, and the quality of life (public comfort) etc. Therefore, it is of utmost importance to take these issues into account especially for those cities like Istanbul with a fast pace of growth. Within the scope of the current study, the spatiotemporal variations in the status of LULC and the skin temperatures of the Istanbul metropolitan area were investigated. The analysis culminated in high accordance between the spatial and temporal interactions of urbanization and UHI intensity which manifests the direct link between the urban development and its negative impacts on the city environment. The authors suggest the decision-makers to take the results of the current study into consideration in their policymaking regarding the urban planning and development in Istanbul. It is also suggested to take adequate measures about mitigating the harsh environmental impacts of the increased skin temperatures especially in the downtown area which suffers the most from the severe UHI phenomenon in Istanbul.

Authors' contributions Behnam Khorrami: conceptualization and methodology, data collation/analysis, writing; Hadi Beygi Heidarlou: methodology, analysis, writing; Bakhtiar Feizizadeh: conceptualization and editing.

Data availability Data used in this study are available to submit upon reasonable request.

Compliance with ethical standards

Competing interests The authors declare that they have no competing interests.

Code availability Not applicable.

References

Akar Ö, Güngör O (2012) Classification of multispectral images using random forest algorithm. J. Geod 1(2):105–112

Alfraihat R, Mulugeta G, Gala T (2016) Ecological evaluation of urban heat island in Chicago City, USA. J Atmos Pollut 4(1):23–29

Amiri R, Weng Q, Alimohammadi A, Alavipanah SK (2009) Spatial–temporal dynamics of land surface temperature in relation to fractional vegetation cover and land use/cover in the Tabriz urban area, Iran. Remote Sens Environ 113(12):2606–2617

Balçik FB (2014) Determining the impact of urban components on land surface temperature of Istanbul by using remote sensing indices. Environ Monit Assess 186(2):859–872

Baumann M, Ozdogan M, Kuemmerle T, Wendland KJ, Esipova E, Radeloff VC (2012) Using the Landsat record to detect forest-cover changes during and after the collapse of the Soviet Union in the temperate zone of European Russia. Remote Sens Environ 124: 174–184

Baumann M, Radeloff VC, Avedian V, Kuemmerle T (2015) Land-use change in the Caucasus during and after the Nagorno-Karabakh conflict. Reg Environ Chang 15:1703–1716

Beygi Heidarlou H, Banj Shafiei A, Erfanian M, Tayyebi A, Alijanpour A (2019) Effects of preservation policy on land use changes in Iranian northern Zagros forests. Land Use Policy 81:76–90

Beygi Heidarlou H, Banj Shafiei A, Erfanian M, Tayyebi A, Alijanpour A (2020) Land cover changes in northern Zagros forests (NW Iran) before and during implementation of energy policies. J Sustain For: 1–15

Breiman, L., 1999, Random forests—random features. Technical Report 567, Statistics Department, University of California, Berkeley, ftp://ftp.stat.berkeley.edu/pub/users/breiman

Cakir G, Ün C, Baskent E, Köse S, Sivrikaya F, Keleş S (2008) Evaluating urbanization, fragmentation and land use/land cover change pattern in Istanbul city, Turkey from 1971 to 2002. Land Degrad Dev 19(6):663–675

Carlson TN, Arthur ST (2000) The impact of land use—land cover changes due to urbanization on surface microclimate and hydrology: a satellite perspective. Glob Planet Chang 25(1–2):49–65

Chen XL, Zhao HM, Li PX, Yin ZY (2006) Remote sensing image-based analysis of the relationship between urban heat island and land use/cover changes. Remote Sens Environ 104(2):133–146

CHEN T, SUN A, NIU R (2019) Effect of land cover fractions on changes in surface urban Heat Islands using Landsat time-series images. Int J Environ Res Public Health 16(6):971

Chun B, Guldmann J-M (2014) Spatial statistical analysis and simulation of the urban heat island in high-density central cities. Landsc Urban Plan 125:76–88

Coulter LL, Stow DA, Tsai Y-H, Ibanez N, Shih H-C, Kerr A, Benza M, Weeks JR, Mensah F (2016) Classification and assessment of land cover and land use change in southern Ghana using dense stacks of Landsat 7 ETM+ imagery. Remote Sens Environ 184:396–409

Dissanayake D, Morimoto T, Ranagalage M, Murayama Y (2019) Land-use/land-cover changes and their impact on surface urban heat islands: case study of Kandy City, Sri Lanka. Climate 7(8):99

Elliot T, Almenar JB, Rugani B (2020) Modelling the relationships between urban land cover change and local climate regulation to estimate urban heat island effect. Urban For Urban Green 126650

Ewing RH, Pendall R, Chen DD (2002) Measuring sprawl and its impact (Vol. 1, p. 55). Smart Growth America, Washington, DC

Geymen A, Baz I (2008) Monitoring urban growth and detecting land-cover changes on the Istanbul metropolitan area. Environ Monit Assess 136(1–3):449–459

GROVER A, SINGH RB (2015) Analysis of urban heat island (UHI) in relation to normalized difference vegetation index (NDVI): a comparative study of Delhi and Mumbai. Environments 2(2):125–138

Haas J (2016) Remote sensing of urbanization and environmental impacts. Doctoral dissertation, KTH Royal Institute of Technology

Hulley GC, Hook SJ (2010) Generating consistent land surface temperature and emissivity products between ASTER and MODIS data for earth science research. IEEE Trans Geosci Remote Sens 49(4): 1304–1315

Imhoff ML, Zhang P, Wolfe RE, Bounoua L (2010) Remote sensing of the urban heat island effect across biomes in the continental USA. Remote Sens Environ 114(3):504–513

Karaburun A, Demirci A, Suen I-S (2010) Impacts of urban growth on forest cover in Istanbul (1987–2007). Environ Monit Assess 166(1–4):267–277

Khorrami B, Gunduz O (2020) Spatio-temporal interactions of surface urban heat island and its spectral indicators: a case study from Istanbul metropolitan area, Turkey. Environ Monit Assess 192: 386. https://doi.org/10.1007/s10661-020-08322-1

Khorrami B, Gunduz O, Patel N, Ghouzlane S, Najjar M (2019) Land surface temperature anomalies in response to changes in forest cover. Int. j. eng. geosci 4(3):149–156

KOTHARKAR R, SURAWAR M (2016) Land use, land cover, and population density impact on the formation of canopy urban heat islands through traverse survey in the Nagpur urban area, India. J Urban Plan Dev 142(1):04015003

Kuang W, Chi W, Lu D, Dou Y (2014) A comparative analysis of megacity expansions in China and the US: patterns, rates and driving forces. Landsc Urban Plan 132:121–135

Lemus-Canovas M, Martin-Vide J, Moreno-Garcia MC, Lopez-Bustins JA (2020) Estimating Barcelona's metropolitan daytime hot and cold poles using Landsat-8 land surface temperature. Sci Total Environ 699:134307

Li ZL, Becker F (1993) Feasibility of land surface temperature and emissivity determination from AVHRR data. Remote Sens Environ 43(1):67–85

Li J, Song C, Cao LU, Zhu F, Meng X, Wu J (2011) Impacts of landscape structure on surface urban heat islands: a case study of Shanghai, China. Remote Sens Environ 115(12):3249–3263

Luyssaert S, Jammet M, Stoy PC, Estel S, Pongratz J, Ceschia E, Churkina G, Don A, Erb K, Ferlicoq M (2014) Land management and land-cover change have impacts of similar magnitude on surface temperature. Nat Clim Chang 4(5):389–393

Malik MS, Shukla JP, Mishra S (2019) Relationship of LST, NDBI and NDVI using Landsat-8 data in Kandaihimmat watershed. Hoshangabad, India

Mallick J, Kant Y, Bharath B (2008) Estimation of land surface temperature over Delhi using Landsat-7 ETM+. J Indian Geophys Un 12(3):131–140

Meineke EK, Dunn RR, Frank SD (2014) Early pest development and loss of biological control are associated with urban warming. Biol Lett 10(11):20140586

Myint SW, Wentz EA, Brazel AJ, Quattrochi DA (2013) The impact of distinct anthropogenic and vegetation features on urban warming. Landsc Ecol 28(5):959–978

Naghibi SA, Pourghasemi HR, Dixon B (2016) GIS-based groundwater potential mapping using boosted regression tree, classification and regression tree, and random forest machine learning models in Iran. Environ Monit Assess 188(1):44

OECD (2018). Rethinking urban sprawl: moving towards sustainable cities. ORGANIZATION FOR ECONOMIC. https://www.oecd-ilibrary.org/sites/9789264189881-5-en/index.html?itemId=/content/component/9789264189881-5-en#An3.A

Olofsson P, Foody GM, Stehman SV, Woodcock CE (2013) Making better use of accuracy data in land change studies: estimating accuracy and area and quantifying uncertainty using stratified estimation. Remote Sens Environ 129:122–131

Pal M (2005) Random forest classifier for remote sensing classification. Int J Remote Sens 26(1):217–222

Pal S, Akoma OC (2009) Water scarcity in wetland area within Kandi block of West Bengal: a hydro-ecological assessment. Ethiop. J Environ Stud Mgmt 2(3)

Pal S, Ziaul S (2017) Detection of land use and land cover change and land surface temperature in English bazar urban centre. Egypt J Remote Sens Space Sci 20(1):125–145

Parastatidis D, Mitraka Z, Chrysoulakis N, Abrams M (2017) Online global land surface temperature estimation from Landsat. Remote Sens 9(12):1208

Plocoste T, Jacoby-Koaly S, Molinié J, PETIT R (2014) Evidence of the effect of an urban heat island on air quality near a landfill. Urban Clim 10:745–757

Ren P, Zhang X, Liang H, Meng Q (2019) Assessing the impact of land cover changes on surface urban heat islands with high-spatial-resolution imagery on a local scale: workflow and case study. Sustainability 11(19):5188

Renard F, Alonso L, Fitts Y, Hadjiosif A, Comby J (2019) Evaluation of the effect of urban redevelopment on surface urban heat islands. Remote Sens 11(3):299

Rizwan AM, Dennis LY, Chunho L (2008) A review on the generation, determination and mitigation of urban heat island. J Environ Sci 20(1):120–128

Salih M, Jasim O, Hassoon K, Abdalkadhum A (2018) Land surface temperature retrieval from LANDSAT-8 thermal infrared sensor data and validation with infrared thermometer camera. Int. J. Eng. Technol 7(4.20):608–612

Schell CJ (2018) Urban evolutionary ecology and the potential benefits of implementing genomics. J Hered 109(2):138–151

Sensoy, S., Demircan, M., Ulupinar, Y., Balta, İ. (2008). Climate of Turkey. Turkish state meteorological service, 401. https://www.researchgate.net/publication/296597022_Climate_of_Turkey. Accessed: 10.05.2020

Sobrino J, Jiménez-Muñoz J, Sòria G, Ruescas A, Danne O, Brockmann C, Ghent D, Remedios J, North P, Merchant C (2016) Synergistic use of MERIS and AATSR as a proxy for estimating land surface temperature from Sentinel-3 data. Remote Sens Environ 179:149–161

Song DX, Huang C, Sexton JO, Channan S, Feng M, Townshend JR (2015) Use of Landsat and corona data for mapping forest cover change from the mid-1960s to 2000s: case studies from the eastern United States and Central Brazil. ISPRS J Photogramm Remote Sens 103:81–92

Steyven, A., Hart, E., Paechter, B. 2018. An investigation of environmental influence on the benefits of adaptation mechanisms in evolutionary swarm robotics. In Proceedings of the Genetic and Evolutionary Computation Conference, pp. 155-162

Sun H, Forsythe W, Waters N (2007) Modeling urban land use change and urban sprawl: Calgary, Alberta, Canada. Netw Spat Econ 7(4): 353–376

Tarakyanet,2019. Population Istatistics of Istanbul. Accessed October 2, https://trakyanet.com/istatistikler/nufus/yillara-gore-nufus/yillara-gore-nufus-istanbul.html

Tran DX, Pla F, Latorre-Carmona P, Myint SW, Caetano M, Kieu HV (2017) Characterizing the relationship between land use land cover change and land surface temperature. ISPRS J Photogramm Remote Sens 124:119–132

Tsendbazar N-E, de Bruin S, Mora B, Schouten L, Herold M (2016) Comparative assessment of thematic accuracy of GLC maps for specific applications using existing reference data. Int J Appl Earth Obs Geoinf 44:124–135

Turkish State Meteorological Service (TSMS) (2020) Official statistics, Annual temperature and precipitation data of Istanbul. https://www.mgm.gov.tr/veridegerlendirme/il-ve-ilceler-istatistik.aspx?k=undefined&m=ISTANBUL. Accessed 15 May

UNITED NATIONS (2010) World urbanization prospects: the 2009 revision. Population Division, Department of Economic and Social Affairs, New York, USA

Wang K, Liang S (2009) Evaluation of ASTER and MODIS land surface temperature and emissivity products using long-term surface longwave radiation observations at SURFRAD sites. Remote Sens Environ 113(7):1556–1565

Wang, S., Xiang, M., He, Y., Tsou, J., Zhang, Y., San Liang, X., & Lu, X. (2018). Evaluating urban heat island effects in rapidly developing coastal cities. In coastal environment, disaster, and infrastructure-a case study of China's coastline Intech Open. DOI: https://doi.org/10.5772/intechopen.80020. Available at: https://www.intechopen.com/books/coastal-environment-disaster-and-infrastructure-a-case-study-of-china-s-coastline/evaluating-urban-heat-island-effects-in-rapidly-developing-coastal-cities

Zhang H, Qi ZF, Ye XY, Cai YB, Ma WC, Chen MN (2013) Analysis of land use/land cover change, population shift, and their effects on spatiotemporal patterns of urban heat islands in metropolitan Shanghai, China. Appl Geogr 44:121–133